

Supporting Information for the paper

Highly Efficient Polarization of Spin-1/2 Insensitive NMR Nuclei by Adiabatic Passage through Level Anti-Crossings

*Andrey N. Pravdivtsev,^{†,‡} Alexandra V. Yurkovskaya,^{†,‡} Nikita N. Lukzen,^{†,‡} Konstantin L.
Ivanov,^{†,‡,*} Hans-Martin Vieth[§]*

[†] International Tomography Center, Institutskaya 3a, Novosibirsk, 630090, Russia

[‡] Novosibirsk State University, Pirogova 2, Novosibirsk, 630090, Russia

[§] Institut für Experimentalphysik, Freie Universität Berlin Arnimallee 14, Berlin, 14195,
Germany

*** Corresponding Author**

E-mail: ivanov@tomo.nsc.ru. Tel. +7-383-330-8868. Fax +7-383-333-1399

Sample preparation and experimental detail. In experiments we used a 5 mm NMR tube with 700 μl of acetone- d_6 as a solvent with variable amount of the substrate, dimethyl acetylenedicarboxylate (purchased from Sigma Aldrich), and the catalyst, 1,4-Bis(diphenylphosphino)butane(1,5-cyclooctadiene)Rh(I) tetrafluoroborate (purchased in ABCR GmbH & Co.). We used 230 mM of the substrate and 2 mM of the catalyst for some of repeated measurements because in this case the experiment can be performed approximately 70 times without a significant loss of polarization. The best signal enhancement in a single-shot experiment (all substrate molecules are into the product in one experiment) was obtained for a sample with 4.7 mM of the substrate and 30 mM of the catalyst. Experiments were done at a 400 MHz NMR spectrometer. Bubbling by *para*- H_2 was performed at a high field of the NMR spectrometer. A plastic capillary was inserted into a 5 mm NMR tube with the sample. The thickness and diameter of the capillary were chosen in such a way that the change of the NMR linewidth was negligible and the size of gas bubbles was much less than the inner diameter of the tube. The pressure of gas in the capillary was adjusted to get uniform distribution of tiny bubbles in the sample. All bubbles in the sample disappear during the time period of less than 0.3 s when the H_2 supply is stopped. In experiments we used the time period of $\tau_b = 9$ s for bubbling and the time period of $\tau_r = 0.5$ s after bubbling and before applying the RF-excitation is (see Figure 1 in the main text).

Calculation method. Let us now explain the form of the Hamiltonian in the DRF given by eqn. (1) in the main text. First, let us write the Hamiltonian in the laboratory frame in the presence of two RF-fields:

$$\begin{aligned} \hat{H}_{lf} = & -2\nu_1^H(\hat{I}_{1x} + \hat{I}_{2x}) \cos(2\pi\nu_{rf}^H t) - \nu_H(\hat{I}_{1z} + \hat{I}_{2z}) - 2\nu_1^C \hat{F}_x \cos(2\pi\nu_{rf}^C t) - \nu_C \hat{F}_z + \\ & J_{HH}(\hat{\mathbf{I}}_1 \cdot \hat{\mathbf{I}}_2) + J_1(\hat{\mathbf{I}}_1 \cdot \hat{\mathbf{F}}) + J_2(\hat{\mathbf{I}}_2 \cdot \hat{\mathbf{F}}) \end{aligned} \quad (1S)$$

Thus, the Hamiltonian takes into account the interaction of protons and carbon with the external field and also with the oscillating RF-fields; the scalar spin-spin couplings are also taken into account. Transition to the rotating frame is required to get rid of the time-dependent terms; in our case it is necessary to apply rotation for both protons and carbons. To go to the rotating frame for protons one should apply the following operator: $\hat{R}_H = \exp[2\pi i \nu_{rf}^H (\hat{I}_{1z} + \hat{I}_{2z}) t]$ to modify the Hamiltonian:

$$\hat{H}_{lf} \rightarrow \hat{R}_H^{-1} \hat{H}_{lf} \hat{R}_H \quad (2S)$$

After that, rotation should also be applied for the carbon nucleus; the following operator should be then used: $\hat{R}_C = \exp[2\pi i \nu_{rf}^C \hat{F}_{1z} t]$. The resulting Hamiltonian is as follows:

$$\hat{H}_{arf} = \hat{R}_C^{-1} \{ \hat{R}_H^{-1} \hat{H}_{lf} \hat{R}_H \} \hat{R}_C \quad (3S)$$

It is important to note that this Hamiltonian still has time-dependent terms. However, terms oscillating with frequencies ν_H^{rf} , $2\nu_H^{rf}$, ν_C^{rf} , $2\nu_C^{rf}$ and $(\nu_H^{rf} \pm \nu_C^{rf})$ are far off-resonance, i.e., they cannot induce transitions between the spin levels. For this reason, they can be neglected in the Hamiltonian, which then takes the form given by eqn. (1).

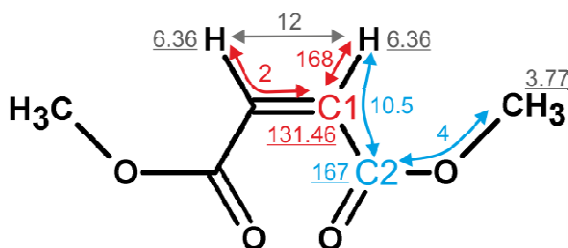
To describe the resulting spin order we calculated the density matrix of the spin system. As initial condition we have taken the density matrix, $\hat{\rho}_a$, which describes the singlet-state preparation of the protons originating from parahydrogen and zero polarization for the carbon spin. After that, we calculated the variation of this density matrix under the action of switched

RF_C-field by numerically solving the Liouville-von Neumann equation with time-dependent Hamiltonian. Using the resulting density matrix, $\hat{\rho}_b$, spin magnetization, M_z , of the carbon nucleus was calculated as the expectation values of the corresponding spin operator:

$$M_z = \text{Tr}\{\hat{F}_z \hat{\rho}_b\} \quad (4S)$$

This calculation scheme is known to be reasonably fast and precise to describe polarization transfer effects in PHIP and its recent off-spring SABRE.

Calculations were run with NMR parameters given in Chart 1S.



Maleic acid dimethyl ester

CHART 1S. NMR parameters of maleic acid dimethyl ester. Chemical shifts (underlined) are assigned to specific nuclei; spin-spin interactions (in Hz) are written on top of the corresponding doubles arrow connecting spins.

Time dependence of carbon polarization. Dependence of polarization on τ_{off} for C1 and C2 is given in Figure 1S. It is seen that the dependence for the C1 carbon has a maximum at certain τ_{off} ; the dependence for C2 saturates at long τ_{off} . In the absence of relaxation both dependences should go to a constant value at very long τ_{off} . This is because the long switching time guarantees that the adiabatic conditions are fulfilled; consequently, re-distribution of non-thermal spin order proceeds in accordance with the theoretical consideration presented in the main text. However, in reality, at very long τ_{off} there is an overall decay of spin order due to spin relaxation. For this reason, a compromise should be found between the time (i) long enough to provide adiabaticity and (ii) short enough to minimize relaxation losses; i.e., there is an

optimal value of τ_{off} for each carbon position. For the C1 position with shorter relaxation time the optimal τ_{off} value is equal to 0.5 s and the corresponding NMR enhancement is equal to 6,400. For the C2 position the τ_{off} dependence reaches a plateau and saturates at about 12 s; the maximal enhancement is then about 2,500. The reason why adiabaticity is easier to fulfill (i.e., the enhancement grows faster with τ_{off}) for the C1 position than for the C2 position is the larger proton-carbon spin-spin interactions in the system with C1 as compared to the case of C2.

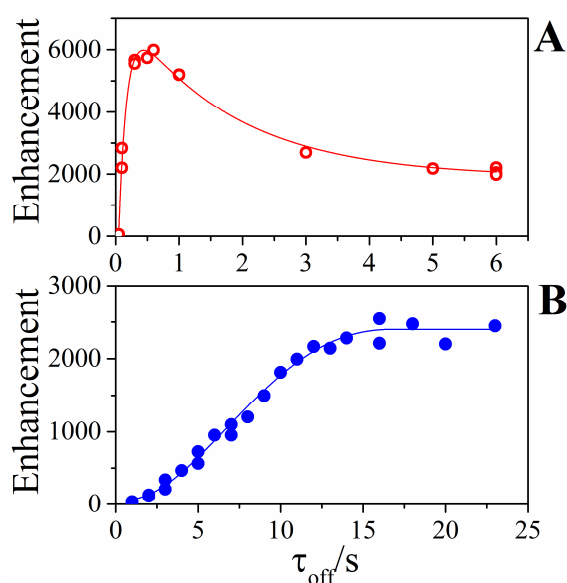


FIGURE 1S. Dependence of carbon polarization on the time τ_{off} of switching the RF_C -field. In (A) the results are shown for C1 obtained with $\nu_{rf}^C=134$ ppm; in (B) the results are shown for C2 obtained with $\nu_{rf}^C=173$ ppm. The strength of the RF_H -field was 2600 Hz and the initial strength of the RF_C -field was slightly higher. Lines are drawn only to guide the eye.

LAC positions and transfer pathways. The sign of the carbon polarization depends on the LACs, which are passed during the switch of the RF_C -field. In turn, these LACs depend on the parameters of the two RF-fields; since in our case the parameters of the RF_H -field were always kept the same, different LACs are exploited depending on the amplitude, ν_1^C , and frequency, ν_{rf}^C , of the RF_C -field.

Here we present the energy levels in both spin systems under study, comprising the two protons originating from para-H₂ and each of the two carbons. As is mentioned in the main text, LACs in these two systems are different: in the case of C1 there is a large proton-carbon coupling present, which results in the formation of triple LACs, whereas in the C2 case there are two isolated LACs instead.

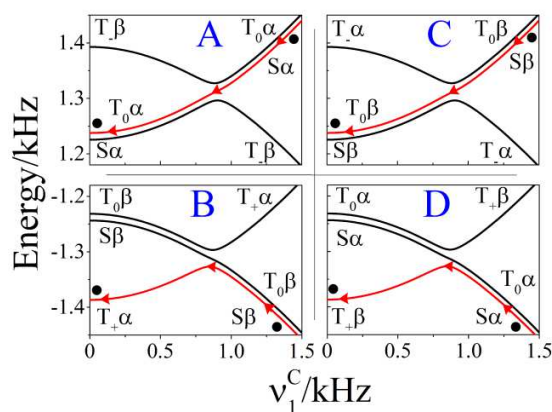


FIGURE 2S. Energy levels of the three-spin system comprising the C1 carbon as a function of ν_1^c . Here $\nu_1^H = 2600$ Hz, $\nu_{rf}^H = 6.36$ ppm; for (A, B) $\nu_{rf}^c = 155.92$ ppm; for (C, D) $\nu_{rf}^c = 107$ ppm. Arrows show the pathway of population re-distribution in the system upon decreasing ν_1^c ; black balls show the population of the levels before and after passing through the LACs. The populated adiabatic level is shown in red.

The energy level diagrams for the three-spin system comprising the C1 carbon are shown in Figure 2S. Here two cases are considered, of positive and negative $\delta\nu_C$. For each case we show the three energy levels in two manifolds. In these manifolds, far away from LACs, the eigenstates of the system are (in the DRDTF): $T_+\beta$, $T_0\alpha$, $S\alpha$ and $T_-\alpha$, $T_0\beta$, $S\beta$. In both manifolds there are triple LACs clearly seen when the proton and carbon frequencies are matched in the DRDTF. In subfigures A and B of Figure 2S a positive value of $\delta\nu_C$ is chosen; in this case there are two adiabatic transitions occurring upon passage through the triple LAC: $S\alpha \rightarrow T_0\alpha$ and $S\beta \rightarrow T_+\alpha$. Thus, for the initial $S\alpha$ -state the carbon spin state stays the same, whereas for the $S\beta$ -state the carbon spin flips; consequently, the singlet spin order of the two protons is converted into positive net polarization of the carbon spin. In the case of negative $\delta\nu_C$, which corresponds

to subfigures C and D of Figure 2S, the spin transitions occurring upon adiabatic passage through the LAC are: $S\beta \rightarrow T_0\beta$ and $S\alpha \rightarrow T_+\beta$. Consequently, negative polarization of the carbon is formed.

The energy level diagrams for the three-spin system comprising the C2 carbon are shown in Figure 3S. Again, here two cases are shown, of positive and negative $\delta\nu_C$. Since the proton-proton coupling is the largest in the system there are two isolated LACs (crossings of T_0 and T_\pm and of S and T_\pm) instead of the single triple LAC, as is shown in Figure 2S. Despite the different appearance of the level diagram the spin mixing occurs in the same way as before when the Hamiltonian is changed in an adiabatic way. For positive $\delta\nu_C$ (subfigures A and B of Figure 3S) the transitions are: $S\alpha \rightarrow T_0\alpha$ and $S\beta \rightarrow T_+\alpha$. Consequently, the carbon spin acquires positive net polarization. In the case of negative $\delta\nu_C$ (see subfigures C and D of Figure 3S) the spin transitions are: $S\beta \rightarrow T_0\beta$ and $S\alpha \rightarrow T_+\beta$ and negative net polarization of the carbon is formed.

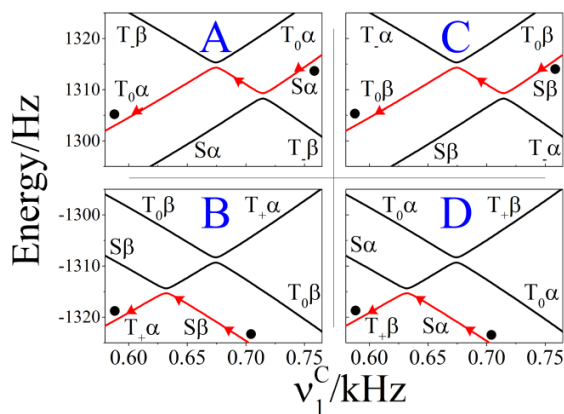


FIGURE 3S. Energy levels of the three-spin system in case of C2 as a function of ν_1^C . Here $\nu_1^H = 2600$ Hz, $\nu_{rf}^H = 6.36$ ppm; for (A, B) $\nu_{rf}^C = 192$ ppm; for (C, D) $\nu_{rf}^C = 142$ ppm. Arrows show the pathway of population redistribution in the system upon decreasing ν_1^C ; black balls show the population of the levels before and after passing through the LACs. The populated adiabatic level is shown in red.

In addition, we demonstrate how the energy levels change upon variation of ν_{rf}^C instead of ν_1^C , see Figures 4S and 5S. For the three-spin system comprising the C1 carbon, see Figure 4S, there

are also triple LACs in each of the two manifolds. When the system with the C2 carbon is considered, there are two isolated LACs. Thus, the same LACs can be accessed not only by varying the RF_C -field strength at a fixed frequency but also by varying the frequency at fixed RF_C -field amplitude. In this work, we pursued only the first option, which is technically easier and was shown to provide high efficiency of polarizing the carbon nuclei.

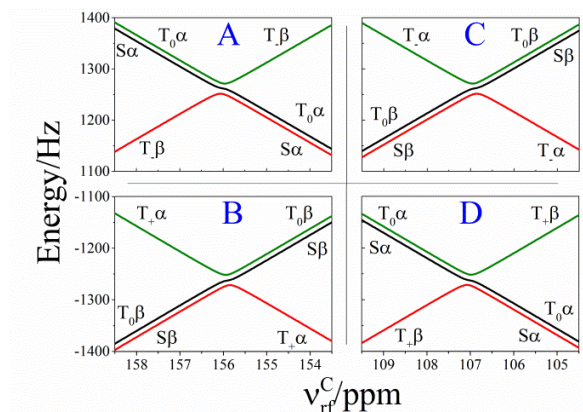


FIGURE 4S. Energy levels of the three-spin system in the case of the C1 carbon as a function of v_{rf}^C . Here $v_1^H = 2600$ Hz, $v_{rf}^H = 6.36$ ppm, $v_1^C = 500$ Hz. For (A, B) $\delta v_C > 0$, for (C, D) $\delta v_C < 0$.

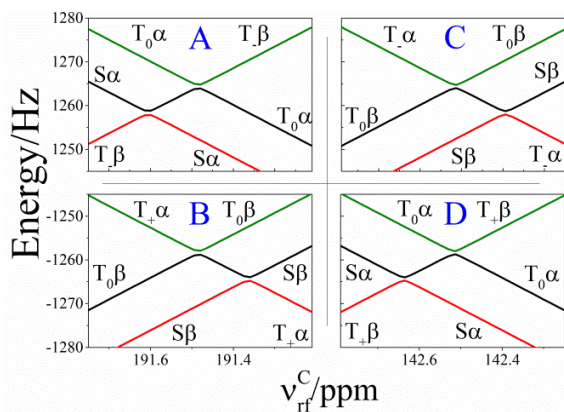


FIGURE 5S. Energy levels of the three-spin system in the case of the C1 carbon as a function of v_{rf}^C . Here $v_1^H = 2600$ Hz, $v_{rf}^H = 6.36$ ppm, $v_1^C = 500$ Hz. For (A, B) $\delta v_C > 0$, for (C, D) $\delta v_C < 0$.

REFERENCES

1. Adams, R. W.; Aguilar, J. A.; Atkinson, K. D.; Cowley, M. J.; Elliott, P. I.; Duckett, S. B.; Green, G. G.; Khazal, I. G.; Lopez-Serrano, J.; Williamson, D. C. Reversible Interactions with Para-Hydrogen Enhance NMR Sensitivity by Polarization Transfer. *Science* **2009**, *323*, 1708-1711.
2. Day, S. E.; Kettunen, M. I.; Gallagher, F. A.; Hu, D. E.; Lerche, M.; Wolber, J.; Golman, K.; Ardenkjaer-Larsen, J. H.; Brindle, K. M. Detecting Tumor Response to Treatment Using Hyperpolarized ^{13}C Magnetic Resonance Imaging and Spectroscopy. *Nature Med.* **2007**, *13*, 1382-1387.
3. Frydman, L.; Blazina, D. Ultrafast Two-Dimensional Nuclear Magnetic Resonance Spectroscopy of Hyperpolarized Solutions. *Nature Phys.* **2007**, *3*, 415-419.
4. Griesinger, C.; Bennati, M.; Vieth, H.-M.; Luchinat, C.; Parigi, G.; Höfer, P.; Engelke, F.; Glaser, S. J.; Denysenkov, V.; Prisner, T. F. Dynamic Nuclear Polarization at High Magnetic Fields in Liquids. *Prog. Nucl. Magn. Reson. Spectr.* **2012**, *64*, 4-28.
5. Schröder, L.; Lowery, T. J.; Hilty, C.; Wemmer, D. E.; Pines, A. Molecular Imaging Using a Targeted Magnetic Resonance Hyperpolarized Biosensor. *Science* **2006**, *314*, 446-449.
6. Theis, T.; Ganssle, P.; Kervern, G.; Knappe, S.; Kitching, J.; Ledbetter, M. P.; Budker, D.; Pines, A. Parahydrogen-Enhanced Zero-Field Nuclear Magnetic Resonance. *Nature Phys.* **2011**, *7*, 571-575.
7. Maly, T.; Debelouchina, G. T.; Bajaj, V. S.; Hu, K.-N.; Joo, C.-G.; Mak-Jurkauskas, M. L.; Sirigiri, J. R.; van der Wel, P. C. A.; Herzfeld, J.; Temkin, R. J.; Griffin, R. G. Dynamic Nuclear Polarization at High Magnetic Fields. *J. Chem. Phys.* **2008**, *128*, 052211.
8. Lelli, M.; Gajan, D.; Lesage, A.; Caporini, M. A.; Vitzthum, V.; Mieville, P.; Heroguel, F.; Rascon, F.; Roussey, A.; Thieuleux, C.; Boualleg, M.; Veyre, L.; Bodenhausen, G.; Coperet, C.; Emsley, L. Fast Characterization of Functionalized Silica Materials by Silicon-29 Surface Enhanced NMR Spectroscopy Using Dynamic Nuclear Polarization. *J. Amer. Chem. Soc.* **2011**, *133*, 2104-2107.
9. Lee, J. H.; Okuno, Y.; Cavagnero, S. Sensitivity Enhancement in Solution NMR: Emerging Ideas and New Frontiers. *J. Magn. Reson.* **2014**, *241*, 18-31.
10. Natterer, J.; Bargon, J. Parahydrogen induced polarization. *Prog. Nucl. Magn. Reson. Spectr.* **1997**, *31*, 293-315.
11. Green, R. A.; Adams, R. W.; Duckett, S. B.; Mewis, R. E.; Williamson, D. C.; Green, G. G. R. The Theory and Practice of Hyperpolarization in Magnetic Resonance Using Parahydrogen. *Prog. Nucl. Magn. Reson. Spectr.* **2012**, *67*, 1-48.
12. Goldman, M.; Jóhannesson, H.; Axelsson, O.; Karlsson, M. Design and Implementation of C-13 Hyperpolarization From Para-Hydrogen, for New MRI Contrast Agents. *C. R. Chim.* **2006**, *9*, 357-363.
13. Franzoni, M. B.; Buljubasich, L.; Spiess, H.-W.; Münnemann, K. Long-Lived ^1H Singlet Spin States Originating from Para-Hydrogen in Cs-symmetric Molecules Stored for Minutes in High Magnetic Fields. *J. Amer. Chem. Soc.* **2012**, *134*, 10393-10396.
14. Plaumann, M.; Bommerich, U.; Trantzsche, T.; Lego, D.; Dillenberger, S.; Sauer, G.; Bargon, J.; Buntkowsky, G.; Bernarding, J. Parahydrogen-Induced Polarization Transfer to ^{19}F in Perfluorocarbons for ^{19}F NMR Spectroscopy and MRI. *Chem. Eur. J.* **2013**, *19*, 6334-6339.

15. Dechent, J. F.; Buljubasich, L.; Schreiber, L. M.; Spiess, H. W.; Münnemann, K. Proton Magnetic Resonance Imaging with Para-Hydrogen Induced Polarization. *Phys. Chem. Chem. Phys.* **2012**, *14*, 2346-2352.
16. Hamans, B. C.; Andreychenko, A.; Heerschap, A.; Wijmenga, S. S.; Tessari, M. NMR at Earth's Magnetic Field Using Para-Hydrogen Induced Polarization. *J. Magn. Reson.* **2011**, *212*, 224-228.
17. Glöggler, S.; Colell, J.; Appelt, S. Para-Hydrogen Perspectives in Hyperpolarized NMR. *J. Magn. Reson.* **2013**, *235*, 130-142.
18. Aguilar, J. A.; Elliott, P. I. P.; Lopez-Serrano, J.; Adams, R. W.; Duckett, S. B. Only Para-Hydrogen Spectroscopy (OPSY), a Technique for the Selective Observation of Para-Hydrogen Enhanced NMR Signals. *Chem. Commun.* **2007**, 1183-1185.
19. Cai, C.; Coffey, A. M.; Shchepin, R. V.; Chekmenev, E. Y.; Waddell, K. W. Efficient Transformation of Parahydrogen Spin Order into Heteronuclear Magnetization. *J. Phys. Chem. B* **2013**, *117*, 1219-1224.
20. Chekmenev, E. Y.; Norton, V. A.; Weitekamp, D. P.; Bhattacharya, P. Hyperpolarized H-1 NMR Employing Low Gamma Nucleus for Spin Polarization Storage. *J. Amer. Chem. Soc.* **2009**, *131*, 3164-3165.
21. Roth, M.; Koch, A.; Kindervater, P.; Bargon, J.; Spiess, H. W.; Münnemann, K. ¹³C Hyperpolarization of a Barbituric Acid Derivative via Parahydrogen Induced Polarization. *J. Magn. Reson.* **2010**, *204*, 50-55.
22. DeVience, S. J.; Walsworth, R. L.; Rosen, M. S. Preparation of Nuclear Spin Singlet States Using Spin-Lock Induced Crossing. *Phys. Rev. Lett.* **2013**, *111*, 173002.
23. Theis, T.; Feng, Y.; Wu, T.; Warren, W. S. Composite and Shaped Pulses for Efficient and Robust Pumping of Disconnected Eigenstates in Magnetic Resonance. *J. Chem. Phys.* **2014**, *140*, 014201.
24. Jóhannesson, H.; Axelsson, O.; Karlsson, M. Transfer of Para-Hydrogen Spin Order into Polarization by Diabatic Field Cycling. *C. R. Phys.* **2004**, *5*, 315-324.
25. Kiryutin, A. S.; Yurkovskaya, A. V.; Kaptein, R.; Vieth, H.-M.; Ivanov, K. L. Evidence for Coherent Transfer of Para-Hydrogen Induced Polarization at Low Magnetic Fields. *J. Phys. Chem. Lett.* **2013**, *4*, 2514-2519.
26. Miesel, K.; Ivanov, K. L.; Yurkovskaya, A. V.; Vieth, H.-M. Coherence Transfer During Field-Cycling NMR Experiments. *Chem. Phys. Lett.* **2006**, *425*, 71-76.
27. Franzoni, M. B.; Graafen, D.; Buljubasich, L.; Schreiber, L. M.; Spiess, H. W.; Münnemann, K. Hyperpolarized ¹H Long Lived States Originating from Parahydrogen Accessed by RF Irradiation. *Phys. Chem. Chem. Phys.* **2013**, *15*, 17233-17239.
28. Pravdivtsev, A. N.; Yurkovskaya, A. V.; Lukzen, N. N.; Vieth, H.-M.; Ivanov, K. L. Exploiting Level Anti-Crossings (LACs) in the Rotating Frame for Transferring Spin Hyperpolarization. *Phys. Chem. Chem. Phys.* **2014**, *16*, 18707-18719.
29. Kiryutin, A. S.; Ivanov, K. L.; Yurkovskaya, A. V.; Vieth, H.-M.; Lukzen, N. N. Manipulating Spin Hyper-Polarization by Means of Adiabatic Switching of RF-Field. *Phys. Chem. Chem. Phys.* **2013**, *15*, 14248-14255.
30. Hediger, S.; Meier, B. H.; Kurur, N. D.; Bodenhausen, G.; Ernst, R. R. NMR Cross Polarization by Adiabatic Passage through the Hartmann-Hahn Condition (APHH). *Chem. Phys. Lett.* **1994**, *223*, 283-288.
31. Pelupessy, P.; Chiarparin, E. Hartmann-Hahn Polarization Transfer in Liquids: An Ideal Tool for Selective Experiments. *Concepts Magn. Reson.* **2000**, *12*, 103-124.

32. Buljubasich, L.; Franzoni, M. B.; Spiess, H. W.; Münnemann, K. Level Anti-Crossings in Parahydrogen Induced Polarization Experiments with Cs-Symmetric Molecules. *J. Magn. Reson.* **2012**, *219*, 33-40.
33. Levitt, M. H.; Freeman, R.; Frenkiel, T. Broadband Heteronuclear Decoupling. *J. Magn. Reson. (1969)* **1982**, *47*, 328-330.
34. Pravdivtsev, A. N.; Yurkovskaya, A. V.; Kaptein, R.; Miesel, K.; Vieth, H.-M.; Ivanov, K. L. Exploiting Level Anti-Crossings for Efficient and Selective Transfer of Hyperpolarization in Coupled Nuclear Spin Systems. *Phys. Chem. Chem. Phys.* **2013**, *15*, 14660-14669.